ChemSusChem

Research Article
doi.org/10.1002/cssc.202200804

Chemistry Europe
European Chemical Societies Publishing

www.chemsuschem.org

Molecular Metallocorrole–Nanorod Photocatalytic System for Sustainable Hydrogen Production

Kaituo Dong[+],[a] Trung-Anh Le[+],[a] Yifat Nakibli,[a] Alexander Schleusener,[b, c] Maria Wächtler,[b, c, d] and Lilac Amirav*[a]

Solar-driven photocatalytic generation of hydrogen from water is a potential source of clean and renewable fuel. Yet systems that are sufficiently stable and efficient for practical use have not been realized. Here, nanorod photocatalysts that have proven record activity for the water reduction half reaction were successfully combined with molecular metallocorroles suitable for catalyzing the accompanying oxidation reactions. Utilization of OH^-/•OH redox species as charge transfer shuttle between freely mixed metallocorroles and rods resulted in quantum efficiency that peaked as high as 17% for hydrogen production from water in the absence of sacrificial hole scavengers. While typically each sacrificial scavenger is able to extract but a single hole, here the molecular metallocorrole catalysts were found to successfully handle nearly 300,000 holes during their lifespan. The implications of the new system on the prospects of realizing practical overall water splitting and direct solar-to-fuel energy conversion were discussed.

Introduction

The solar-driven photocatalytic splitting of water into hydrogen and oxygen is potentially the most ideal source of clean and renewable fuel; yet systems that are sufficiently stable and efficient for practical use have not been realized. One significant milestone towards this goal was accomplished with the demonstration of a perfect 100% photon-to-hydrogen production efficiency. This record activity in promoting the photocatalytic water reduction half reaction was obtained via utilization of a well-controlled nanoparticle-based system.[1,2] It is composed of a platinum-tipped cadmium sulfide (CdS) rod with an embedded cadmium selenide seed (CdSe),[3–5] with architecture that facilitates an efficient long-lasting charge carrier separation,[6] and the formation of distinct and spatially segregated reaction sites for the different redox half reactions. A single Pt-CdSe@CdS rod can produce 360000 molecules of hydrogen per hour. Unfortunately, this system is not suitable for overall water splitting as it is hampered by photochemical instability. Prolonged irradiation of its suspensions leads to photocorrosion, and it therefore requires the use of sacrificial electron donors (hole scavengers) for photochemical H_2 evolution from water.

Given the demanding set of requirements for proper selection of a semiconductor system that can support visible light water splitting (e.g., suitable bandgap and electron affinity), and the fact that CdS is among the few materials that meet these strict requirements, addressing CdS stability is of outmost importance. The addition of a second co-catalyst such as IrO_2[7,8] or Ru[9] that can scavenge the holes from the semiconductor and mediate their transfer to water was shown to afford CdS-based structures the desired photochemical stability. Yet these co-catalysts did not support a sustainable oxidation process. Hence, finding an appropriate catalyst that would be able to scavenge the holes from the CdS-based rods, and successfully utilizes the charge for an oxidation half reaction, is of great interest. In this work, molecular catalysts were selected for promoting the oxidation side, and their successful incorporation with the Pt-CdSe@CdS photocatalytic system led to hydrogen production in the absence of sacrificial electron donors.

Combinations of CdS nanorods with molecular catalysts supporting an oxidation reaction were proposed and examined previously. Dukovic and co-workers described the charge transfer interactions between photoexcited CdS nanorods and [Ru-

[a] Dr. K. Dong,[+] T.-A. Le,[+] Dr. Y. Nakibli, Prof. L. Amirav
Schulich Faculty of Chemistry
Technion – Israel Institute of Technology
Haifa 32000 (Israel)
and
Current address of T.-A. Le:
Faculty of science and engineering
Åbo Akademi University
Turku 20500 (Finland)
E-mail: lilac@technion.ac.il
Homepage: http://www.amiravlab.com
[b] Dr. A. Schleusener, Dr. M. Wächtler
Leibniz Institute of Photonic Technology
Albert-Einstein-Straße 9, 07745 Jena (Germany)
and
Current address of Dr. A. Schleusener:
Istituto Italiano di Tecnologia
Via Morego 30, 16163 Genova (Italy)
[c] Dr. A. Schleusener, Dr. M. Wächtler
Institute of Physical Chemistry
Friedrich Schiller University Jena
Helmholtzweg 4, 07743 Jena (Germany)
[d] Dr. M. Wächtler
Abbe Center of Photonics
Albert-Einstein-Straße 6, 07745 Jena (Germany)
[+] These authors contributed equally to this work.

Supporting information for this article is available on the WWW under https://doi.org/10.1002/cssc.202200804

(deeb)(tpy)Cl](PF$_6$) water oxidation catalyst and determined that the metal center (within the molecular catalyst) acts as a recombination site.[10] They proposed that this could be averted through introduction of additional electron harvesting pathways. The addition of Pt at the tip of the rods is expected to be beneficial in this regard. In a separate later study, Dukovic and co-workers concluded that the ultrafast hole transfer from CdS quantum dots to the ruthenium-based water oxidation catalyst directly competes with hole trapping at the CdS surface.[11] This limits the efficiency of hole harvesting even if the surface is saturated with catalysts. Note that such surface saturation with the oxidation catalysts might not be advantageous for multi-electron reactions.[12]

A conceptually similar principle has been demonstrated with a Pt-tipped CdS nanorod system functionalized with a molecular Ru(tpy)(bpy)Cl$_2$-based oxidation catalyst, which was reported to support simultaneous H_2 and O_2 evolution.[13] Yet, O_2 was not produced with stoichiometric ratio, the overall efficiency of the process was limited to 0.1–0.27%, and the system lost its activity after only 1–2 h of operation. Based on the data provided, a turnover number (TON) for the molecular catalysts is calculated to be between 134 and 466. That is, the molecular catalyst was found to scavenge merely 466 holes before it was deactivated. This low activity may be rationalized by incomplete hole transfer from the CdS to the molecular catalyst, and coupling methodology (i.e., the use of a linker for direct immobilization of the catalyst) that might prevent the required accumulation of several holes on a single molecular oxidation site, or even act as a hole trap.

Thus, the development of systems that will further improve upon these critical steps and enable efficient removal of photoexcited holes from CdS to non-sacrificial oxidation catalysts requires revisiting the system design and coupling methodology. Herein we demonstrate that the limitations of direct coupling of the molecular catalysts to CdS structures may be avoided altogether when redox species act as charge transfer shuttle and close the cycle between freely mixed components.

Interesting candidates in this respect are metallocorrole complexes, consisting of a metal center and a corrole-based ligand.[14–16] Their capacity to support and stabilize both (unusually) high and low formal oxidation states of the coordinated metal ion[17,18] encouraged exploration of their potential in serving as catalysts for both fuel cells and batteries, supporting oxygen evolution or reduction reactions.[19–24] In this work, metallocorrole molecular catalysts were selected for promoting the oxidation side in an overall water-splitting process, and their successful coupling to the Pt-CdSe@CdS photocatalytic system led to stable hydrogen production in the absence of sacrificial electron donors.

Results and Discussion

Conceptually, direct connection of metallocorroles onto the nanorod surface using a linker that enables charge transfer between the two components would be an elegant approach. In practice, however, this might involve highly challenging chemistry, considering that we are interested in anchoring only a single catalyst, and at a precise location around the encapsulated CdSe seed. Moreover, the linker must enable directional charge transfer of holes from the semiconductor to the molecular metallocorrole catalyst, while maintaining stability under irradiation, oxidative and reductive conditions, and at a wide pH range. The linkers of interest should possess a group such as monodentate thiolate or dithiocarbamate that would enable strong binding to the CdS surface on one side, with a coordinating functional group that can chelate to the metal site in metallocorroles on their other side. The linker should successfully chelate to the metal center or corrole skeleton of the metallocorroles, while avoiding deactivation of the catalyst towards water oxidation as a result of blocked coordinating sites. While we believe in the merits of a direct linker that can support and sustain charge transfer between the semiconductor photosensitizer and the molecular catalyst, the aforementioned challenges, which are inherent to the design and the specific system studied here, led us to examine alternative strategies.

Rather than having a direct charge transfer via linkers, we examined utilization of redox species as charge transfer shuttles. Amphiphilic corrole complexes were prepared and mixed with the nanorod photocatalysts under high pH conditions. For full information on corrole and nanorods synthetic procedures and characterization, the reader is referred to the Supporting Information, Experimental Section 1 and 2, including Figures S1–S17. In the complete system presented herein the CdSe@CdS rod serve as the light excitation-unit, and photoinduced electrons are transferred to the platinum tip, which serve as the reduction site on which hydrogen is generated. After being briefly localized in the CdSe seed, photoinduced holes are transferred to the metallocorrole via OH^-/$^\bullet$OH redox species that operate as charge transfer shuttles between freely mixed corroles and rods, as illustrated in Figure 1. According to this proposed mechanism the rods oxidize OH^- to $^\bullet$OH radical upon illumination, which in turn

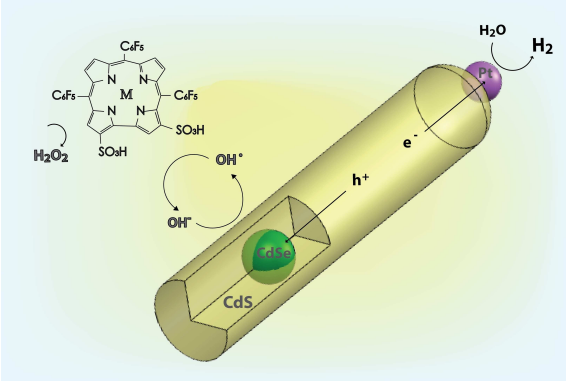

Figure 1. Illustration of the photocatalytic CdSe@CdS-Pt rod and a metallocorrole, with proposed mechanism that is based on charge transfer via OH^-/$^\bullet$OH redox species.

may oxidize the metallocorrole, thus completing one charge transfer cycle.

First, we evaluated the activity of the photocatalytic rods towards hydrogen production, when combined with metallocorroles in such fashion, and in the absence of the molecular catalyst. It is well established that the activity on the reduction side also reflects on trends in the oxidation side (as the latter were identified as the bottleneck of the complete process). Control experiments (not shown) demonstrate that (1) corroles alone (i.e., without rods as light sensitizers) cannot support the photocatalytic reaction, indicating that the corroles are not photoactive; and (2) operation under neutral conditions, that is, without OH^-/•OH redox species serving as charge transfer shuttle, resulted in only negligible H_2 production, indicating the shuttles' vital role.

Different sets of Pt-decorated CdSe@CdS nanorods were examined in the course of this work, and results are presented here for rods that were around 45–50 nm long with 2.3 nm seed size. Metallocorrole complexes containing different metal centers were examined in combination with the rods, and various concentrations were examined as well. Complexes of naturally abundant 3d transition metals, such as Mn, Fe, and Cu, are of particular interest due to practical availability and their redox modulating activity and were the focus of the present work.[25–29] Additionally, a Ga based metallocorrole was used. These were compared with the activity and long-term stability of rods in the absence of metallocorrole, and any sacrificial hole scavengers.

Solutions containing about 5×10^{14} rods and varying type and amount of corroles, all suspended in 10 mL water at basic (pH 14) conditions, were placed in a custom-built gas-tight reaction cell purged with argon (Figure S19). The samples were then illuminated with a 455 nm LED adjusted to 50 mW (equivalent to a photon flux of $N_{h\nu}$ 1.15×10^{17} photons/sec^{-1}). The evolving hydrogen was analyzed using an online gas chromatograph (GC) equipped with a thermal conductivity detector (TCD). Operation in continuous-flow mode allowed for direct determination of the gas production rate (N_{H_2}). The apparent quantum efficiency (QE) of the sample is defined according to Equation (1):

$$\mathrm{QE} = \frac{2N_{H_2}}{N_{h\nu}} \quad (1)$$

It was determined by quantifying the amount of evolved hydrogen at a given photon flux. Following the changes in the H_2 production rate over time is equivalent to direct monitoring of the QE time trajectories, and this offers insights into the dynamic processes that may take place during operation, for example, on the surface of the photocatalyst.

The temporal development of the photocatalytic quantum efficiency towards hydrogen production obtained for mixtures of rods and Ga- (purple), Mn- (blue), Cu- (light blue), and Fe-based (green) corrole complexes is presented in Figure 2, alongside the control sample of rods without corroles (yellow) as supporting oxidizing catalyst. Close monitoring of the quantum efficiency for H_2 evolution over time revels maxima

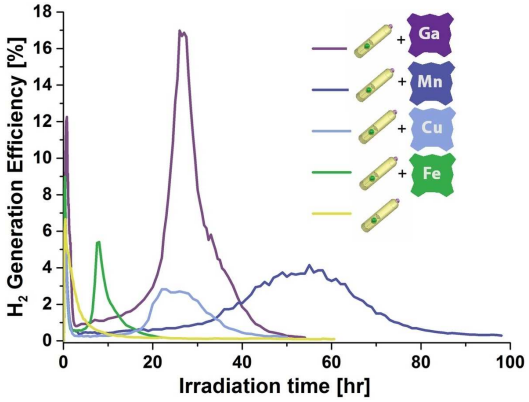

Figure 2. Activities towards photocatalytic hydrogen production obtained from CdSe@CdS-Pt rods that are combined with corrole complexes with Ga (purple), Mn (blue), Cu (light blue), or Fe (green) as the metal center, or no corroles at all (yellow). Excitation with 50 mW, 455 nm LED; $\approx5\times10^{14}$ rods (8.6×10^{-10} mol and 86 nM); metallocorrole concentration 428 nM.

that are obtained within the first minutes of the measurement, followed by an activity drop and finally a second buildup of the efficiency. The first short-lived spike in activity is ascribed to consumption of residual methanol, or excess free ligands, from the ligand exchange procedure. Hence, we refer in this work only to the operation values that developed later on. Oxygen production was not detected in the course of this work with neither of the applied metallocorroles. The TON for the molecular catalysts was calculated as the ratio between the total amount of holes that are produced by the rods over the entire life cycle of the system (determined as double the amount of H_2 molecules), and the amount of metallocorroles in the solution. It reflects the ability of the molecular catalysts to scavenge holes in continuous manner, thus supporting sustainable hydrogen production. Full details are provided in the Supporting Information, in section 4.3, Figure S20.

In all of the investigated systems an induction time was observed, that is, the activity towards hydrogen production was slowly developing over time. We note that a similar induction time, on the order of about 20 h until full activity is reached, was previously reported for this metal-tipped photocatalyst system, while operating in the presence of sacrificial hole scavengers such as isopropyl alcohol (IPA). It was proposed that this induction time is the outcome of reorganization of the ligands on the photocatalyst surface.[30] In other words, modifications that influence mostly the kinetics of hole transfer to the solution. Herein, the various metal centers seem to influence the characteristics of this latent activity buildup. Hence, the observed latency is attributed to a combination of the typical induction period, and the kinetics of the oxidation reactions promoted by the metallocorroles that complete the redox cycle. The dependency of the induction time on the presence of the metallocorroles and type of metal center that is employed is attributed to the different kinetics of the oxidation cycle under these conditions. Note that in the absence of metallocorroles, the activity never develops (as will be discussed later).

Rods mixed with Fe based metallocorrole display the fastest buildup of their activity, yet the maximum that is obtained within 9 h is also accompanied by the shortest stability (up to 20 h). On the other hand, rods mixed with Mn-based metallocorroles demonstrated slow and steady increase of the efficiency during nearly 45 h of illumination and maintained stable activity of around 3.8% for additional nearly 20 h, before a gradual drop in activity is observed again. Cu- and Ga-based metallocorroles display activity development characteristics that are between those observed for Fe and Mn. The differences in activity between the various metal centers signify of the complete system's sensitivity towards the quality of the molecular catalyst. Yet, since utilization of metal complexes other than cobalt corroles as catalysts for oxygen evolution reaction (OER) is relatively nascent,[14,31] we can only speculate on the underlying mechanism, and detailed explanation of the observed trends call for further work. The activity of the complex with gallium, Ga(tpfc)$(SO_3H)_2$, came as a surprise since metal-centered redox reactions are not possible for it.[32] We note however the report by Shiragamia et al., who showed that other post-transition metal complexes (germanium porphyrins in their case) may catalyze the oxidation of water to hydrogen peroxide.[33] The key reaction intermediate is a hydroxy/germanium-coordinated porphyrin radical, which is in perfect analogy to what may be expected to result from the combination of hydroxyl radicals with gallium corroles.

The final drop in hydrogen production, which is observed for all of the investigated systems, is attributed to a drop in metallocorrole activity, and the resulting poisoning of the rods by accumulation of •OH radicals that are no longer scavenged by the corroles. In addition, it is suggested that accumulated damage from the potential oxidation reaction byproduct (H_2O_2) also contributes to the rods' degradation (see further discussion later on). A faster kinetics for hole scavenging by the metallocorrole results in faster formation of the harmful oxidation byproduct, which eventually leads to faster degradation of the rods; hence, a faster drop follows a faster raise of activity. This analysis of individual temporal development trends for hydrogen production is further supported when different metallocorroles are compared. Interestingly, the amount of holes scavenged by both Ga- and Mn-based metallocorroles up to the time upon which maximal QE for H_2 production is attained is nearly identical ($\approx 6.7\times10^{-4}$ and 6.2×10^{-4} mol, respectively; Figure S21). This absolute amount is not influenced by the vastly different temporal development trends displayed, and the fact it takes the Ga-based metallocorrole only around 25 h to establish maximal activity, in comparison with the Mn metallocorrole that requires around 50 h. This finding implies a similar ability of the two metallocorroles to handle holes, despite the variations in oxidation kinetics. Total amounts of H_2 that are produced over time are presented in Figure S22.

These trajectories in activity behavior over time are in sharp contrast to the control sample of rods operating in pure water without the presence of metallocorroles (Figure 2, in yellow), where a somewhat slow initial drop in activity was observed over the course of the first 5–10 h, never to recover again. This fast and complete loss of activity results in only a negligible accumulated amount of H_2 that is obtained from rods in the absence of the metallocorroles, and it is attributed to the open redox cycle. In the absence of any sacrificial hole scavengers or oxidative catalysts, the •OH radicals that are produced over the rods are harmful to the CdS-based photocatalyst system. The detrimental effects of the hydroxyl radicals are avoided when metallocorroles are introduced. This is reflected in substantial improvement in both activity (Figure 2) and long-term stability, as seen in Figure 3, which displays transmission electron microscopy (TEM) images of rods after 36 h of continuous illumination in the presence or absence of the metallocorroles. The harsh and severe damage to the rods' structure when corroles are not present to complete the redox cycle is clearly noticeable.

Several findings are of particular significance: (1) With the aid of Mn-corroles the CdS based system was active for nearly 90 h under continuous illumination, and in the absence of sacrificial electron donors (hole scavengers). This exceptionally considerable operation time is over an order of magnitude longer in comparison to that obtained in the absence of the molecular catalyst. This significant long-term stability was highly reproducible, with only minor dependence on the rods used. (2) With the aid of Ga-corroles this hybrid photocatalytic system demonstrated activity that peaked to as high as around 17% for hydrogen production from water (again in the absence of sacrificial additives). (3) The Ga-based metallocorrole demonstrated an impressive catalytic TON of around 292,000 (detailed calculation is provided in section 4.3 of the Supporting Information, Figure S20). For comparison, the well-established mononuclear ruthenium complex [Ru(bda)$(isoq)_2$] is reported to have a TON of 8360.[34]

The catalytic cycle in the hybrid system, described in Figure 1, includes three major processes: (1) The rods' contribution, where absorption of photons in the rods eventually results in production of H_2 and •OH radicals; (2) charge shuttle, which includes the diffusion of these •OH radicals from the rods' surface and towards the metallocorroles; and finally (3) the molecular catalyst side, where •OH radicals react with the metallocorroles, thus completing the charge transfer cycle. After H_2 production was confirmed, and the contribution of the metallocorroles to the rods' activity and durability is estab-

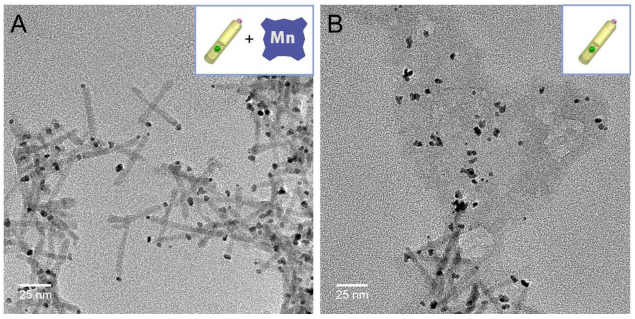

Figure 3. TEM images of rods after 36 h of continuous illumination in the (A) presence or (B) absence of the Mn metallocorroles. The severe damage to the rod's structure is avoided when corroles are introduced. Scale bar: 25 nm.

lished, it is important to confirm formation of •OH radicals by the rods and determine the propensity of the metallocorroles to act as •OH scavengers in a catalytic fashion.

To prove the proposed mechanism, it was first necessary to show independently that metallocorroles are good scavengers of •OH radicals. For this task $Mn(tpfc)(SO_3H)_2$ was selected as a representative metallocorrole. The radicals were generated by mixing under air: 8 μM $CuSO_4$, 8 μM 1,10-phenanthroline, and 500 μM vitamin C in 5 mL Dulbecco's phosphate buffered saline (DPBS) pH 7.4. Formation of •OH was measured in the presence and absence of 200 μM $Mn(tpfc)(SO_3H)_2$ by the terephthalic acid (TPA) probe (500 μM). TPA provides indirect evidence for the existence of •OH radicals. When the nearly non-fluorescent TPA reacts with •OH radicals, the fluorescent 2-hydroxyterephthalic acid (hTPA) is formed. The latter shows a distinctive emission peak at 425 nm upon excitation at 320 nm. A slight emission originating from TPA was also observed, forming a background signal in the recorded emission spectra (Figure S14). The presence of $Mn(tpfc)(SO_3H)_2$ inhibited the production of hTPA by about 86%, indicating reduction in the amount of •OH (Figure S18). Measures were taken to rule out possible decomposition of the radical precursor, H_2O_2, by the $Mn(tpfc)(SO_3H)_2$, as detailed in the Supporting Information. This result proves that the (Mn-based) corroles are good scavengers of •OH. Next, TPA was again used as probe to provide indirect evidence for photocatalytic •OH radical formation upon irradiation of the nanorods at high pH, alongside additional confirmation as per the ability of the $Mn(tpfc)(SO_3H)_2$ metallocorrole to scavenge these radicals in the solution.

Four different TPA probe experiments were performed, and the results are summarized in Figure 4. By carrying out the experiment in the absence of any scavenger, we observed the formation of an emission band at 425 nm over time (Figure 4A), clearly indicating the formation of •OH radicals upon irradiation of the nanorods. This emission band is not formed in the presence of 10 vol% IPA, which is added to the reaction mixture and acts as efficient but sacrificial scavenger (Figure 4B). This is attributed to a fast reaction of •OH radicals with IPA, which prevents the formation of the fluorescent hTPA (or even direct scavenging of holes by the IPA, thus preventing formation of •OH radicals).[35]

Figure 4C,D shows the results of the irradiation experiment with different amounts of added Mn-metallocorrole. For a sample with only low Mn-metallocorrole concentration of 10 nM (Figure 4C), the emission increased over time, similarly to the case where no scavenger was added. In comparison to that, upon increasing the amount of Mn-metallocorrole to 100 nM only a slight rise of the emission over time was observed. This confirms the ability of the Mn-metallocorrole to quench the •OH radicals. The results further indicate that a decrease in the mean distance between nanorod and metallocorrole in the case of a higher molecular catalyst concentration, increases the probability for a reaction between the •OH radical and the Mn-metallocorrole. This finding suggests that the diffusion of the highly reactive •OH radicals from the rods to the corroles is the rate-determining step in the proposed photocatalytic cycle. It is likely that when the •OH radicals have no metallocorroles in their vicinity, they lose their charge by oxidizing the rods, or the hydrogen intermediate, hence jeopardizing the stability and activity of the rods.

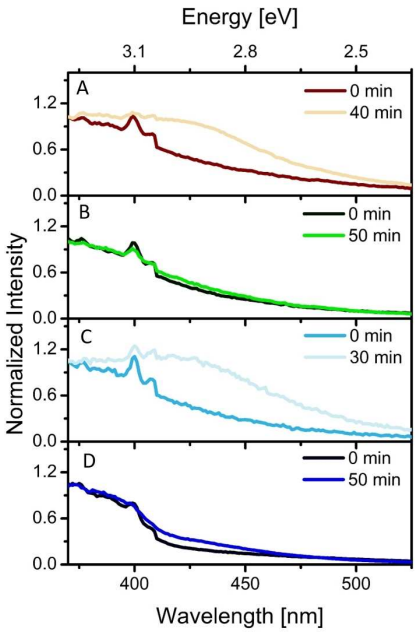

Figure 4. Emission spectra of the TPA probe experiment over time: (A) without adding any hole scavenger, (B) with 10 vol% of isopropanol as sacrificial scavenger, (C,D) with Mn-metallocorrole at low (10 nM) and high (100 nM) concentration respectively. The background at the beginning of the experiment is due to the emission originating from TPA (Figure S14).

To summarize, the ability of the rods to support photocatalytic H_2 production alongside formation of •OH radicals, the migration of the radicals towards the metallocorroles, and their reactivity with the molecular catalyst are confirmed. At this point, better understanding of the role of the charge shuttle's functionally and means for its optimization are desirable, specifically as it appears to the be the rate-determining step. Hence, the activity towards photocatalytic hydrogen production was examined for different corrole concentrations, attempting to increase the corroles amount for maximal catalytic activity. The development of the apparent quantum efficiencies over time, as obtained while mixing different amount of $Mn(tpfc)(SO_3H)_2$ with respect to the rods, is presented in Figure 5.

Utilization of $Mn(tpfc)(SO_3H)_2$ metallocorroles at a concentration of around 85.6 nM (corresponding to 1:1 corrole/rods ratio, plotted in purple) resulted in maximum quantum efficiency for H_2 production of about 4.5%, and overall operation that lasted for nearly 25 h. Raising the corrole concentration by 5-fold (to 428 nM, plotted in blue) led to quite remarkable improvement in terms of stability of the system, and as a result the TON (225,000). Interestingly, rather than simply obtaining a higher efficiency maximum, the recovery of the activity was slower for this higher concentration of corroles.

The mean diffusion path of an •OH radical that is formed on the rods, before it reacts further, can be calculated using Einstein–Smoluchowski diffusion equation based on Brownian motion, and given the concentration of the rods and metal-

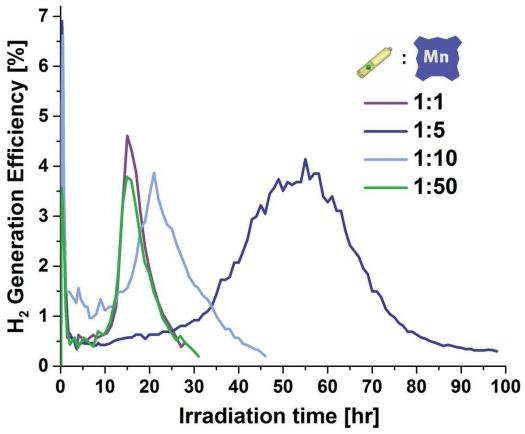

Figure 5. Activities towards photocatalytic hydrogen production obtained from CdSe@CdS-Pt rods that are combined with Mn-based metallocorroles at varied relative ratios. Excitation with 50 mW, 455 nm LED; $\approx 5\times10^{14}$ rods (8.6×10^{-10} mol and 86 nM); corroles concentration: 86 nM (1:1), 428 nM (1:5), 856 nM (1:10), 4280 nM (1:50).

locorroles in the aqueous solution. The detailed calculation is available in the Supporting Information. The mean diffusion length of •OH was calculated to be up to about 150 nm, depending on the reactivity of substrates in the solution. Note that this is an upper cap that neglects numerous alternative reactions. Given a concentration of 5×10^{14} rods in 10 mL (e.g., $\approx$80 nM), and a 1:1 ratio of metallocorroles/rods, the nearest neighbor distance between a metallocorrole molecular catalyst and a rod photocatalyst will be about around 151 nm (for description of the estimation see the Supporting Information). As this distance is just longer than the estimated maximum •OH radical mean diffusion path, there is high probability that the •OH radical will react before finding the molecular catalyst. Further increase of the corroles concentration to a 1:5 ratio of rods/metallocorroles and a concentration of 428 nM, brings the distance to the closest neighbor in the solutions to around 90 nm. For this ratio the redox shuttle is expected to transfer the charge from the rod to the corrole with sufficient likelihood, before the •OH radical will undergo undesired reactions.

To our surprise, further increase in the amount of Mn-corroles present in the reaction cell (to 856 and 4280 nM, plotted in light blue and green accordingly) only resulted in a decrease in the activity displayed by the rods. This behavior, which is non-monotonic with respect to the corroles amount, was reproduced also when aliquots of corroles were added to the reaction cell gradually over time (Figure S23). The drop in activity for higher concentrations of corroles might be attributed to changes in their solubility, and formation of small clusters that might hinder the access of the •OH radicals to the reaction center.[36] An alternative possibility is that the higher corrole concentration increases the chance for direct oxidation of the latter (by the rods), inducing more damage to the catalyst than its metal-centered oxidation by hydroxyl radical.

Yet another interesting alternative explanation for the non-monotonic activity with respect to the corroles amount is based on the possibility that the metallocorroles are directly adsorbed to the surface of the rods or intercalate into the ligand shell. While this will not result in efficient direct charge transfer that bypasses the shuttle (as evident by the negligible activity in neutral conditions), such a scenario will insure a fixed minimal distance the •OH radicals must travel before finding a corrole. Increasing the ratio between metallocorroles and rods increases the possibility for such adsorption or intercalation, while at higher corrole concentrations they may restrict access of water/OH^- to the nanorods' surface.

Achievement of a true catalytic cycle would critically depend on the ability of the metallocorrole to return to its original oxidation state following further reactions. Indeed, as the metallocorroles were found to successfully handle nearly 300000 holes during their lifespan, their functionality as catalysts is confirmed. Yet, several questions still remain open for future study, with the key question related to the specific mechanism of metallocorrole oxidation, which is not accompanied by O_2 evolution. The absence of O_2 formation could in fact be regarded as an advantage, since the evolving hydrogen does not require separation from the oxygen, making this a more economic and safe design. As no oxygen was detected, an alternative product has to be formed. One proposed catalytic cycle for the transition metal corroles (that fits best the case of manganese), includes two separate oxidation steps by •OH radicals, converting the metal center from oxidation state of M^{III} to M^{IV} and finally into M^{V}. In this state the metallocorrole complex can convert to the oxo form,[37] whose stability/reactivity depends very much on the particular metal ion, which can revert back to the original M^{III} state by oxidizing water to hydrogen peroxide (H_2O_2). The other metallocorroles cycle between different redox states but share the ability to reduce the reactive •OH species formed (see below for the case of gallium) during the catalysis.

While water oxidation to O_2 is thermodynamically favorable compared to H_2O_2 production, the latter involves only two electrons rather than four, which potentially results in higher reaction rates.[38–40] Moreover, H_2O_2 was reported to be the dominant product when corroles were employed in homogeneous solutions with limited diffusion (a situation resembling the conditions herein), presumably since under these conditions the oxidation intermediate is hydrolyzed by water, giving H_2O_2 as byproduct, before being oxidized in a manner that will afford O_2 formation.[41] An additional contribution arising from photo-excitation of the corroles cannot be ruled out, potentially facilitating a more thermodynamically tasking route.

Unfortunately, the addition of potassium iodide, which is known to catalyze decomposition of H_2O_2 to O_2 and water, to the reaction cell at the end of a photocatalytic reaction failed to confirm the presence of H_2O_2. Interestingly, a control experiment in which H_2O_2 was deliberately added to a mixture of rods and metallocorroles also showed no traces of H_2O_2. In yet another experiment, rods were tested for photocatalytic production of hydrogen in the presence of IPA as hole scavenger, and the absence of metallocorroles, under pH 14, and demonstrated stable activity (Figure S24A). When H_2O_2 was added to the reaction cell, with amounts equivalent to that expected to be produced by the corroles within 3–4 h, it had a

peculiar and unexpected effect on the photocatalytic activity (Figure S24B). Immediately upon the addition of H_2O_2 the activity towards H_2 production dropped to nearly zero. This is likely due to reduction of the H_2O_2 at the Pt tip, which competes successfully with hydrogen production. Higher catalytic activity results in higher concentrations of H_2O_2, making this reduction pathway more competitive. Once a sufficient concentration of H_2O_2 accumulates, its reduction commences, and this in turn leads to a gradual decrease in H_2 production rate, and eventually stops its production. Such a rise that is followed by a gradual drop in activity fits well with the experimental observations.

In the experiment displayed in Figure S24B, after nearly 0.5 h, the activity not only recovered but also surpassed the original value. Yet this improvement was observed only for the first two cycles, after which further additions of H_2O_2 resulted in permanent damage to the rods (ascertained from their absorption, Figure S25). This observation is in accordance with literature reports, which indicate that reaction between H_2O_2 and CdS nanoparticles first initiates surface passivation, before full oxidation takes place.[42] It is speculated that the significantly longer induction time obtained for rods that are coupled with the Mn metallocorrole, which extend to 50 h, is the result of a slower rate in which H_2O_2 is produced. This enables slow etching of the rod surface, gradually improving activity until the amount of H_2O_2 becomes harmful.

Regardless of the nature of the reaction the H_2O_2 is involved in (reduction at the Pt tip, or oxidation of the CdS rod), it appears it is consumed in situ. It is also reasonable to assume that formation of H_2O_2 by the molecular catalysts slows to a stop towards the end of the metallocorrole lifespan, and hence it cannot be easily detected at the end of a photocatalytic cycle.

The kinetics for H_2O_2 formation by the corroles is accomplished through a mediated reaction cycle and is thus expected to differ from that of the H_2 production at the metal tip, which relies upon direct electron transfer. Hence, H_2 production commences, and proceeds, while H_2O_2 concentration builds up to the critical level that initiates it reduction. A scenario in which H_2O_2 production is detrimental for hydrogen production might explain the somewhat comparable TONs obtained from both Mn- and Ga-based corroles, despite the drastically different time trajectories for efficiency development. Under this assumption, the limitation for a long and lasting activity is accumulation of this byproduct. As mentioned above, a similar amount of H_2O_2 is produced by both metallocorroles, until a sharp drop in activity towards H_2 production is observed. Note that H_2O_2 reduction over the Pt tip is also expected to cap the maximal H_2 production efficiency. The addition of a third catalytic component that can decompose the H_2O_2 in situ might enable mitigation of this limit, affording perfectly stable photocatalytic production of H_2 from water.

Conclusion

A hybrid photocatalytic system composed of CdSe@CdS-Pt rods that are combined with metallocorroles utilizing redox species as a hole transfer shuttle is demonstrated. Photocatalytic hydrogen production quantum efficiency peaks as high as 17%, in the absence of sacrificial hole scavengers. This activity was accompanied by an impressive turnover number of around 292000 for the molecular metallocorrole catalysts. We believe that this work presents a significant step towards realization of solar-to-fuel conversion and successful combination of molecular catalysts with nanoscale semiconductor photocatalysts.

Experimental Section

Confirmation of the formation of photogenerated •OH free radicals

An aqueous solution of 2 mM TPA was mixed with KOH until the pH-value reached 14, and was then degassed by bubbling nitrogen for at least 1 h. Subsequently the solution was transferred to a glovebox and mixed with 300 μL of an aqueous solution of rods (concentration 95 nmol L^{-1}) inside a cuvette to a total volume of 3 mL. Depending on the experiment, different amounts of scavenger [Mn(tpfc)$(SO_3H)_2$ or IPA] were added to the reaction mixture. Afterward the cuvette was sealed and transferred to the outside of the glovebox. The reaction mixture inside the cuvette was irradiated by a 450 nm LED under stirring. The emission was measured after a certain timesteps with a FLS980 spectrometer (Edinburgh Instruments) upon excitation at 320 nm. The weak emission detected from TPA itself is visible in the measurements, due to the low rod concentration and, hence, low amount of •OH radicals produced in the reaction. The concentration was adjusted to result in a low optical density in a 1 cm cuvette to enable the direct measurement of emission spectra without further dilution of the irradiated solution before the measurement.

Experimental setup for hydrogen evaluation

Rods solutions were moved to ultrapure water by mercaptoundecanoic acid (MUA) ligand exchange as close as possible to starting a new measurement, usually less than 1 h before the cell was first purged. Samples were diluted using ultrapure water, after which base and desired amounts of metallocorroles were added to make around 10 mL solutions (pH ≈ 14). The gas-tight reaction cell (Figure S19) was closed and connected to a 10 mL min^{-1} argon line (filtered 99.999% purity) and an Agilent 7890A Series GC-TCD. Gas was continually flowed through the cell in the dark while the solution was stirred, and gas samples were automatically taken every 5 min for measurement to monitor the purging process. When the cell was fully purged, a Thorlabs Royal Blue (455 nm) high-power LED was switched on to illuminate the sample. The photon flux was calculated by measuring the LED power (adjusted to a desired value and measured using a Thorlabs Digital Optical Meter – PM206) assuming all photons had the same wavelength of 455 nm (4.366×10^{-19} J $photon^{-1}$). In this adjustment of the power, we accounted for the irradiated area over the sample as well as for the absorption of the reaction cell window and other minor losses in the setup. The LED power used during this work was 50 mW, thus the photon flux (amounts of photons per second) is 1.15×10^{17} photons s^{-1}.

Acknowledgements

We gratefully acknowledge the vital contribution of Prof. Zeev Gross and Dr. Atif Mahammed. This research was carried out in the framework of the Russell Berrie Nanotechnology Institute (RBNI) and the Nancy and Stephen Grand Technion Energy Program (GTEP). The project received funding from the European Union's Horizon 2020 research and innovation programme under the Marie Skłodowska-Curie grant agreement No 722591, and the Israeli Ministry of National Infrastructures, Energy and Water Resources (grant number 218–11-044). The authors acknowledge the generous funding support from the Fonds der Chemischen Industrie (FCI), the COST Action CM1202 PERSPECT-H_2O, and the German Research Foundation (DFG) project number 364549901-TRR234 (CataLight, B4 and Z2).

Conflict of Interest

The authors declare no conflict of interest.

Data Availability Statement

The data that support the findings of this study are available in the supplementary material of this article.

Keywords: molecular catalysts · nanorods · photocatalysis · solar hydrogen · water splitting

[1] P. Kalisman, Y. Nakibli, L. Amirav, *Nano Lett.* **2016**, *16*, 1776–1781.
[2] L. Amirav, A. P. Alivisatos, *J. Phys. Chem. Lett.* **2010**, *1*, 1051–1054.
[3] D. V. Talapin, R. Koeppe, S. Götzinger, A. Kornowski, J. M. Lupton, A. L. Rogach, O. Benson, J. Feldmann, H. Weller, *Nano Lett.* **2003**, *3*, 1677–1681.
[4] L. Carbone, C. Nobile, M. De Giorgi, F. D. Sala, G. Morello, P. Pompa, M. Hytch, E. Snoeck, A. Fiore, I. R. Franchini, M. Nadasan, A. F. Silvestre, L. Chiodo, S. Kudera, R. Cingolani, R. Krahne, L. Manna, *Nano Lett.* **2007**, *7*, 2942–2950.
[5] D. V. Talapin, J. H. Nelson, E. V. Shevchenko, S. Aloni, B. Sadtler, A. P. Alivisatos, *Nano Lett.* **2007**, *7*, 2951–2959.
[6] L. Amirav, A. P. Alivisatos, *J. Am. Chem. Soc.* **2013**, *135*, 13049–13053.
[7] P. Kalisman, Y. Kauffmann, L. Amirav, *J. Mater. Chem. A* **2015**, *3*, 3261–3265.
[8] P. Kalisman, Y. Nakibli, L. Amirav, *JoVE* **2016**, *108*, e53675.
[9] L. Amirav, F. Oba, S. Aloni, A. P. Alivisatos, *Angew. Chem. Int. Ed.* **2015**, *54*, 7007–7011; *Angew. Chem.* **2015**, *127*, 7113–7117.
[10] H.-W. Tseng, M. B. Wilker, N. H. Damrauer, G. Dukovic, *J. Am. Chem. Soc.* **2013**, *135*, 3383–3386.
[11] O. M. Pearce, J. S. Duncan, N. H. Damrauer, G. Dukovic, *J. Phys. Chem. C* **2018**, *122*, 17559–17565.
[12] Y. Nakibli, P. Kalisman, L. Amirav, *J. Phys. Chem. Lett.* **2015**, *6*, 2265–2268.
[13] C. M. Wolff, P. D. Frischmann, M. Schulze, B. J. Bohn, R. Wein, P. Livadas, M. T. Carlson, F. Jäckel, J. Feldmann, F. Würthner, J. K. Stolarczyk, *Nat. Energy* **2018**, *3*, 862–869.
[14] C. Di Natale, C. P. Gros, R. Paolesse, *Chem. Soc. Rev.* **2022**, *51*, 1277–1335.
[15] I. Aviv-Harel, Z. Gross, *Coord. Chem. Rev.* **2011**, *255*, 717–736.
[16] C. I. M. Santos, J. F. B. Barata, M. J. F. Calvete, L. S. H. P. Vale, D. Dini, M. Meneghetti, M. G. P. M. S. Neves, M. A. F. Faustino, A. C. Tome, J. A. S. Cavaleiro, *Curr. Org. Synth.* **2014**, *11*, 29–41.
[17] Z. Gross, H. B. Gray, *Comments Inorg. Chem.* **2006**, *27*, 61–72.
[18] I. Aviv, Z. Gross, *Chem. Commun.* **2007**, *20*, 1987–1999.
[19] T. Lazarides, T. McCormick, P. Du, G. Luo, B. Lindley, R. Eisenberg, *J. Am. Chem. Soc.* **2009**, *131*, 9192–9194.
[20] H. Lei, X. Li, J. Meng, H. Zheng, W. Zhang, R. Cao, *ACS Catal.* **2019**, *9*, 4320–4344.
[21] Y. Gao, T. Åkermark, J. Liu, L. Sun, B. Åkermark, *J. Am. Chem. Soc.* **2009**, *131*, 8726–8727.
[22] D. K. Dogutan, R. McGuire, D. G. Nocera, *J. Am. Chem. Soc.* **2011**, *133*, 9178–9180.
[23] W.-J. Kwak, A. Mahammed, H. Kim, T. T. Nguyen, Z. Gross, D. Aurbach, Y.-K. Sun, *Mater. Horiz.* **2020**, *7*, 214–222.
[24] H. Lei, Q. Zhang, Z. Liang, H. Guo, Y. Wang, H. Lv, X. Li, W. Zhang, U.-P. Apfel, R. Cao, *Angew. Chem. Int. Ed.* **2022**, *61*, e202201104.
[25] A. Singh, L. Spiccia, *Coord. Chem. Rev.* **2013**, *257*, 2607–2622.
[26] W. Lai, R. Cao, G. Dong, S. Shaik, J. Yao, H. Chen, *J. Phys. Chem. Lett.* **2012**, *3*, 2315–2319.
[27] M. Eckshtain, I. Zilbermann, A. Mahammed, I. Saltsman, Z. Okun, E. Maimon, H. Cohen, D. Meyerstein, Z. Gross, *Dalton Trans.* **2009**, *38*, 7879–7882.
[28] A. Mahammed, Z. Gross, *Chem. Commun.* **2010**, *46*, 7040–7042.
[29] A. Mahammed, Z. Gross, *Angew. Chem. Int. Ed.* **2006**, *45*, 6544–6547; *Angew. Chem.* **2006**, *118*, 6694–6697.
[30] Y. Nakibli, L. Amirav, *Chem. Mater.* **2016**, *28*, 4524–4527.
[31] W. Schöfberger, F. Faschinger, S. Chattopadhyay, S. Bhakta, B. Mondal, J. A. A. W. Elemans, S. Müllegger, S. Tebi, R. Koch, F. Klappenberger, M. Paszkiewicz, J. V. Barth, E. Rauls, H. Aldahhak, W. G. Schmidt, A. Dey, *Angew. Chem. Int. Ed.* **2016**, *55*, 2350–2355; *Angew. Chem.* **2016**, *128*, 2396–2401.
[32] J. Bendix, I. J. Dmochowski, H. B. Gray, A. Mahammed, L. Simkhovich, Z. Gross, *Angew. Chem. Int. Ed.* **2000**, *39*, 4048–4051; *Angew. Chem.* **2000**, *112*, 4214–4217.
[33] T. Shiragami, H. Nakamura, J. Matsumoto, M. Yasuda, Y. Suzuri, H. Tachibana, H. Inoue, *J. Photochem. Photobiol. A* **2015**, *313*, 131–136.
[34] L. Duan, F. Bozoglian, S. Mandal, B. Stewart, T. Privalov, A. Llobet, L. Sun, *Nat. Chem.* **2012**, *4*, 418–423.
[35] T. Simon, N. Bouchonville, M. J. Berr, A. Vaneski, A. Adrović, D. Volbers, R. Wyrwich, M. Döblinger, A. S. Susha, A. L. Rogach, F. Jäckel, J. K. Stolarczyk, J. Feldmann, *Nat. Mater.* **2014**, *13*, 1013–1018.
[36] M. Soll, T. K. Goswami, Q.-C. Chen, I. Saltsman, R. D. Teo, M. Shahgholi, P. Lim, A. J. Di Bilio, S. Cohen, J. Termini, H. B. Gray, Z. Gross, *Sci. Rep.* **2019**, *9*, 2294.
[37] Z. Gross, *Angew. Chem. Int. Ed.* **2008**, *47*, 2737–2739; *Angew. Chem.* **2008**, *120*, 2777–2779.
[38] J. Liu, Y. Zou, B. Jin, K. Zhang, J. H. Park, *ACS Energy Lett.* **2019**, *4*, 3018–3027.
[39] Y. Xue, Y. Wang, Z. Pan, K. Sayama, *Angew. Chem. Int. Ed.* **2021**, *60*, 10469–10480.
[40] J. Liu, Y. Liu, N. Liu, Y. Han, X. Zhang, H. Huang, Y. Lifshitz, S.-T. Lee, J. Zhong, Z. Kang, *Science* **2015**, *347*, 970–974.
[41] B. Mondal, S. Chattopadhyay, S. Dey, A. Mahammed, K. Mittra, A. Rana, Z. Gross, A. Dey, *J. Am. Chem. Soc.* **2020**, *142*, 21040–21049.
[42] W. Lee, H. Kim, D.-R. Jung, J. Kim, C. Nahm, J. Lee, S. Kang, B. Lee, B. Park, *Nanoscale Res. Lett.* **2012**, *7*, 672.

Manuscript received: May 18, 2022
Revised manuscript received: June 30, 2022
Accepted manuscript online: July 5, 2022
Version of record online: July 29, 2022